MICROMETEOROID IMPACTS AND OPTICAL SCATTER IN SPACE ENVIRONMENT

James B. Heaney
Stinger Gaffarian Technologies, 7701 Greenbelt Rd., Greenbelt, MD 20770

Liqin L. Wang and Charles C. He
Ball Aerospace & Technologies Corp., 7404 Executive Place, Lanham, MD 20706

ABSTRACT

This paper discusses the results of an attempt to use laboratory test data and empirically derived models to quantify the degree of surface damage and associated light scattering that might be expected from hypervelocity particle impacts in space environment. Published descriptions of the interplanetary dust environment were used as the sources of particle mass, size, and velocity estimates. Micrometeoroid sizes are predicted to be predominantly in the mass range 10^{-5}g or less, with most having diameters near 1μm, but some larger than 120μm, with velocities near 20km/s. In a laboratory test, latex ($\rho = 1.1$. g/cm^3) and iron (7.9 g/cm^3) particles with diameters ranging from 0.75μm to1.60μm and with velocities ranging from 2.0km/s to 18.5 km/s, were shot at a Be substrate mirror that had a dielectric coated gold reflecting surface. Scanning electron and atomic force microscopy were used to measure crater dimensions that were then associated with particle impact energies. These data were then fitted to empirical models derived from solar cell and other spacecraft surface components returned from orbit, as well as studies of impact craters studied on glassy materials returned from the lunar surface, to establish a link between particle energy and impact crater dimension. From these data, an estimate of total expected damaged area was computed and this result produced an estimate of expected surface scatter from the modeled environment.

INTRODUCTION

Information gleaned from more than 5 decades of space exploration reveals that the likelihood of a space optical system being damaged measurably by micrometeoroid impact is very low. However, examination of hundreds of impact craters found on space hardware returned from missions such as the Long Duration Exposure Facility (LDEF) and the Hubble Space Telescope's (HST) solar panels, or the European Space Agency's European Retrievable Carrier

(EuReCa) also indicate that impact events do occur with harmful consequences.[1-3] With space optical systems growing ever larger , such as the 6m diameter of the James Webb Space Telescope's (JWST) primary mirror that is not buried within a baffling tube, or with planetary missions entering regions of higher dust density, such as the vicinity of Mars or Saturn, the consequences of hypervelocity impact on an optical surface should be addressed. These referenced studies contain measurements of impact crater dimensions that were produced by micrometeoroids of uncertain size, mass, density, and velocity. From these examinations, investigators have constructed somewhat heuristic analytical models that allow users to connect micrometeoroid size and impact energy with expected impact damage dimensions. More recently, actual measured dust particle size, mass, and velocity data have become available from instruments such as the Cosmic Dust Analyzer (CDA) flown aboard the Cassini spacecraft that orbited a good portion of the solar system on its trajectory to Saturn.[4,5] In this report, these measured dust particle parameters are inserted into relevant impact models and to construct the parameters of a hypervelocity impact experiment intended to connect impact crater dimensions with controlled particle size, mass, and velocity. An additional effort was made to augment the analytical models with actual experimental data from a simulated micrometeoroid exposure performed on a gold-coated beryllium substrate test mirror, a replica of the telescope primary mirror of NASA's Composite Infrared Spectrometer (CIRS) instrument aboard the Cassini spacecraft that entered orbit around Saturn in late 2004.[6]

The impact crater dimensions then form the basis of a discussion related to optical surface scatter.

Micrometeoroid Environment

An estimate of the hypervelocity particle flux in near-Earth orbit is provided by a published study of the impact sites found on the front side of the returned HST solar array, as shown on Fig. 1.[1,2] The limited range of measure data in Fig. 1 includes both meteoroids and debris, a

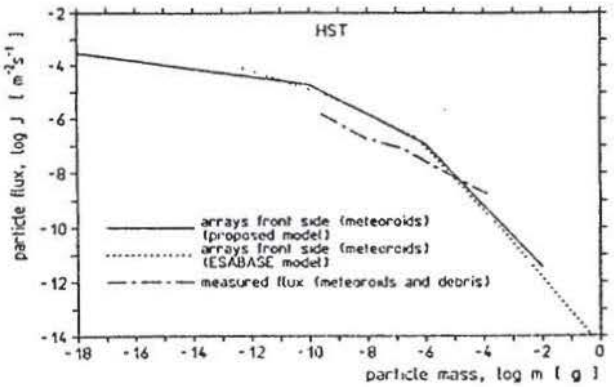

Figure 1. Meteoroid flux on the front side of the retrieved Hubble Space Telescope solar array. (Ref 1)

combination unique to near-Earth orbit. The plot exhibits a leveling tendency for mass below 10^{-10}g and particle fluxes less than 10^{-5} /m^2-s . For the near-Earth environment, but further out than the HST orbit, such as in the vicinity of the L2 libration point that will be occupied by the large JWST mirror, a study edited by S.W. Evans et al. used an earlier model developed by Grün to produce the meteoroid flux estimate presented in Fig. 2.[4,7] The model plotted in Fig. 2 estimates about 10 impacts/m^2-s for particles with mass of $1x10^{-7}$ g. By comparison, the models plotted in Fig. 1, for a 10^{-7}g mass, estimate about 2 to 3 impacts/m^2-s. This may be taken as good agreement in consideration of the uncertainties involved.

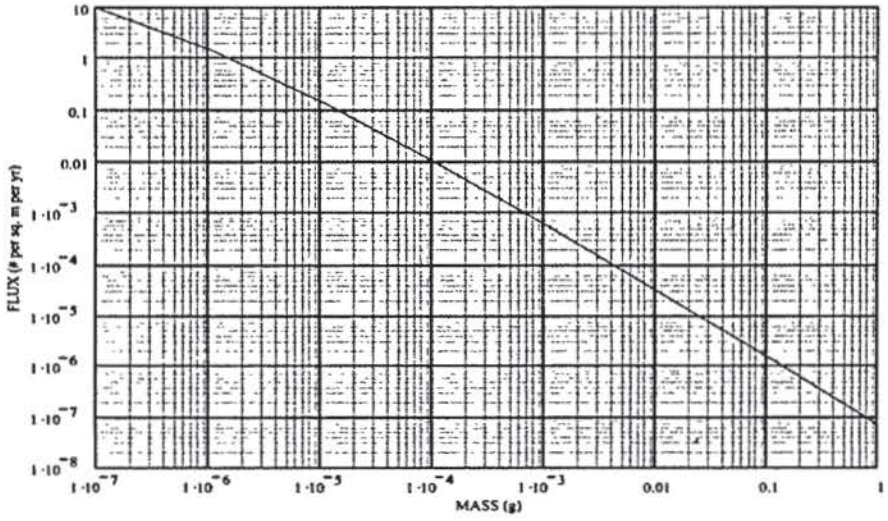

Figure 2. Meteoroid flux as a function of mass as determined by Grün (Ref 4)

Local meteoroid flux in the near-Earth environment, including at L2, can be significantly enhanced by the passage of well-known meteorite occurrences, as identified in Table 1 below.

Table 1 – Known meteorite occurrences that can increase the local background flux.

Stream	Radiant		Speed (km s^{-1})	Time of max activity
	RA	Declination		
Quadrantids	230°	+49°	41	Jan 03
κ Cygnids	286°	+59°	25	Aug. 18
Lyrids	271°	+34°	49	Apr. 22
Draconids	262°	+54°	20	Oct. 09
Perseids	46°	+58°	59	Aug 13
Leonids	152°	+22°	71	Nov. 17-18

Further away from Earth, in interplanetary space, the Cosmic Dust Analyzer (CDA) aboard Cassini on its journey to Saturn recorded 37 impacts in a 3 month period with mass in excess of 10^{-13} kg and velocities generally below 25 km/s, except for a few with smaller mass and higher velocities. Two of these interplanetary dust particles detected by the CDA were iron rich with lesser traces of other elements. The detected masses were in the range 9×10^{-14} kg and 1.4×10^{-12}

kg and, from assumed densities of 7874 – 2500 kg/m^3 , their radii were 0.7μm – 4μm and 2.6μm – 6.8μm respectively.[8]

A specific example of a local micrometeoroid environment that was prepared by the Jet Propulsion Laboratory for a Mars orbiting laser telecommunication instrument will be used as a sample meteoroid background flux.[9] The estimated omnidirectional micrometeoroid fluence in the near-Mars environment, extracted from Ref. 9, is presented in Figure 3 as a function of velocity and mass. (The sharp rises in the curves of Figure 2 at 40km/s are due to the fact that the last data bin includes all predicted micrometeoroids with velocity > 40 km/s.)

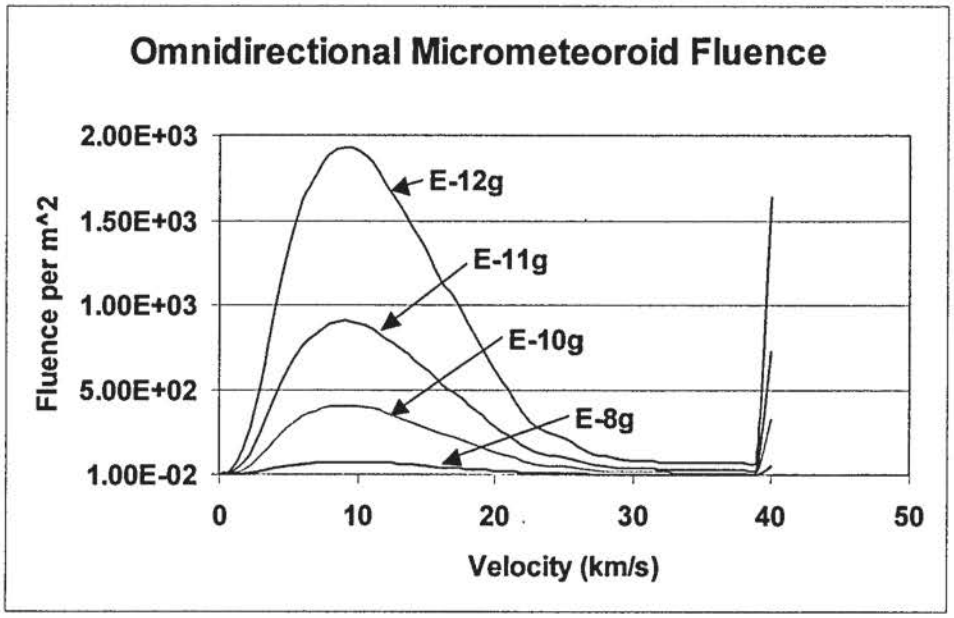

Figure 3 – The omnidirectional micrometeoroid fluence for a 3 year Mars mission, as extracted from the JPL Environmental Requirements Document.[9]

The micrometeoroid environment described in Figure 3 can be used to construct a laboratory experiment in which particles of known diameter, mass, and density can be accelerated to hypervelocities and directed at targets representative of space optical components.

EXPERIMENTAL METHODS

Target Mirror

A cross-sectional sketch of the Be substrate mirror with reflecting protected gold surface that was subjected to hypervelocity particle impact is presented in Fig. 4. The composition of this

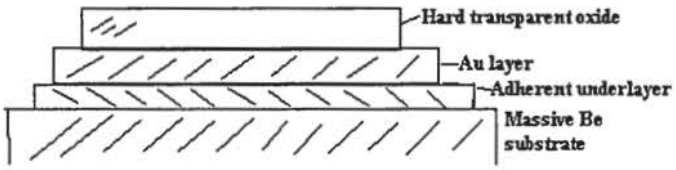

Figure 4. Cross-sectional sketch of the gold on beryllium mirror.

mirror is very similar to that which will be used for the JWST telescope optics. The hard oxide layer is approximately 200nm thick and the gold layer is about 120nm thick.

Hypervelocity Particle Accelerator

A dust particle accelerator at the Max Planck Institute for Nuclear Physics in Heidelberg was used to perform the mirror bombardment tests.[10] This Heidelberg Dust Accelerator facility can generate projectile velocities up to about 40km/s for various materials to simulate interplanetary dust. It contains a 2 MeV electrostatic accelerator with an attached calibrated dust particle source that can supply dust grains with sizes between 0.02μm and 6.0μm. A more complete description of this facility is given in Ref. 10.

During particle bombardment, the test mirror was positioned in the accelerator's high vacuum chamber target area. A mask with a 10mm hole was placed directly in front of a single mirror zone during bombardment with particles of selected material, grain size, and velocity. The mask shielded all other mirror areas during particle exposure. In this manner, discreetly identified mirror portions were exposed sequentially to individual particles of latex ($\rho = 1.1$ g/cm^3) to simulate ice and iron ($\rho = 7.9$ g/cm^3) with sizes ranging from 0.75μm to1.60μm and with velocities ranging from 2.0 km/s to 18.5 km/s.

Crater Dimensioning

Individual impact craters were photographed and dimensioned with a scanning electron microscope (SEM) (Leica Cambrige S360, tungsten filament SEM) operated in the secondary electron detection mode. The accelerating voltage for the images was typically 10 kV, with a beam current of around 40 pA. This microscope was useful when examining flaking of the surface coating in the area surrounding an impact site. Spectroscopic examination of the backscattered x-ray spectra also yielded material composition data that allowed a distinction to be made between the Be substrate and the protected gold overcoat in the vicinity of an impact site. It also detected iron inside the central portion of impact sites created by hypervelocity iron projectiles.

A scanning probe microscope (SPM) (Digital Instruments, Dimension 3000), used in the tapping mode, with silicon probes of radius about 10 nm, was used to produce latex and iron impact

crater dimension, depth, and cross-section profiling images. Typical latex impact craters are presented in Fig. 5 and typical iron impact craters are presented in Fig. 6.

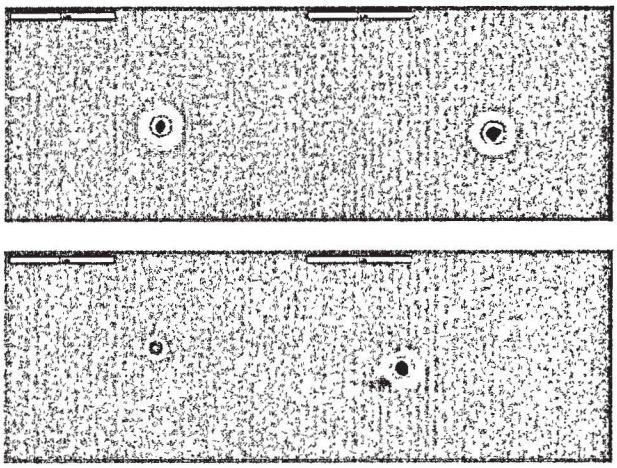

Figure 5. SEM photos of 4 latex impacts. (5μm scale)

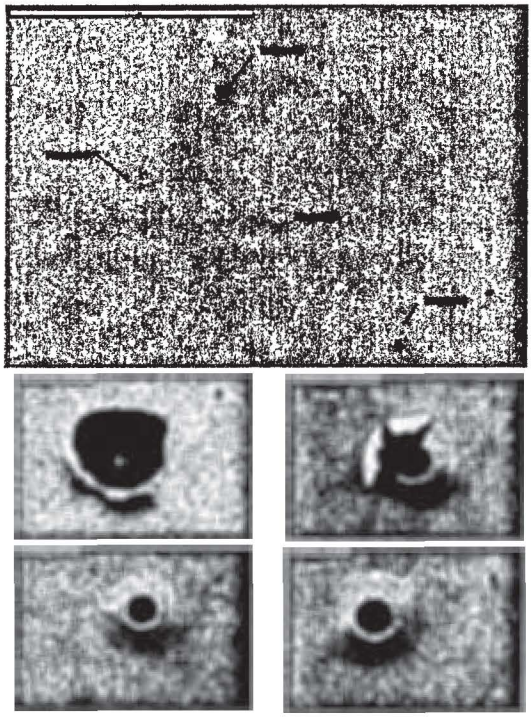

Figure 6. SEM photos of 4 iron impacts. (10μm & 5μm scales)

57 latex impact craters were individually dimensioned using the SEM . Typical latex particle grain size is 0.75μm which corresponds to a mass of about 0.24 x 10^{-15} kg, a value comparable to the mass of the interplanetary dust detected by the Cassini CDA. Impact velocities were in the range 11.5 – 12.5 km/s . The average measured damage diameter was 1.69 ± 0.21μm.

213 iron impact craters were examined. They were produced by iron particles of size 1.17 ± 0.27μm with velocities ranging from 2 to 40 km/s . The average measured damage diameter was 7.36 ± 2.49 μm.

SPM images of typical iron craters are presented in Figure 7. Images such as these were used to dimension the diameter and pit depth of the craters.

These observations produced two relations that connected projectile properties with impact crater dimensions. The first connected projectile kinetic energy with crater diameter (0.1μm/nJ); the second connected crater diameter with particle diameter (damage dia./particle dia. = 2 to 3 for ρ = 1 g/cm3 and 5 – 10 for ρ = 8 g/cm3). These empirically determined results were then

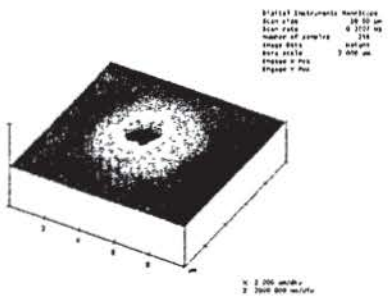

Figure 7a. SPM image of an iron impact crater. Scale extent = 10μm

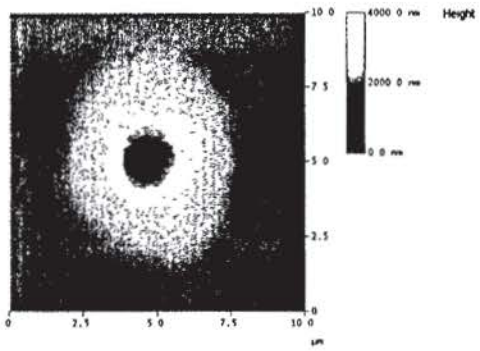

Figure 7b. SPM image of an iron impact crater, 10μm on edge, with 4000nm scale height.

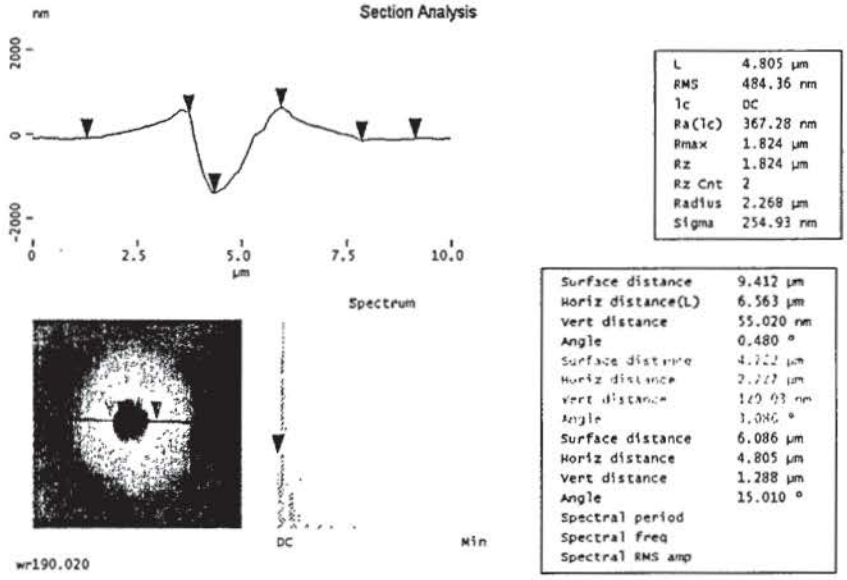

Figure 7c. SPM image of an iron crater with damage diameter 6.6 μm.

compared to crater dimensions computed from published formulae – one that emphasized mass and another that emphasized velocity as the determining parameters.

MODEL COMPARISONS

In order to get an estimate of diameters for the masses of impacting particles, a spherical shape was assumed. There is good evidence from studies of lunar craters and craters in hardware returned from space that impact damage is approximately circular, independent of micrometeoroid shape or incidence angle. Assuming spherical shapes, the computed diameters of expected micrometeoroids are presented in Figure 8 as a function of particle mass.

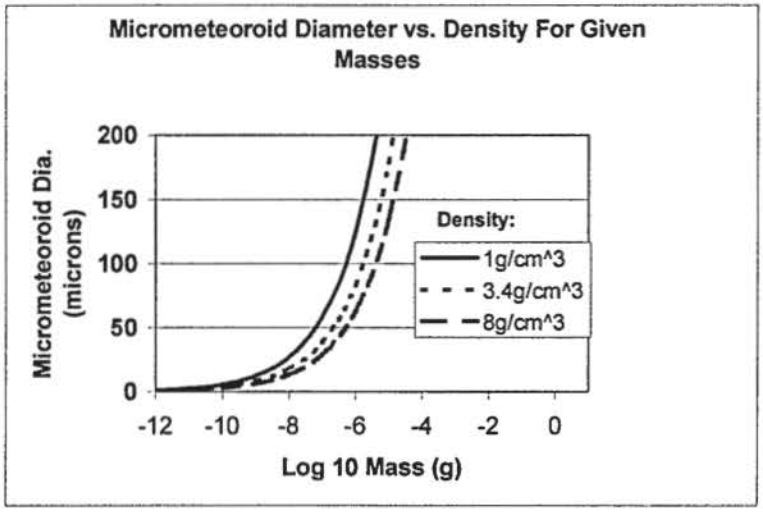

Figure 8. Estimates of micrometeoroid diameter variations for 3 values of assigned likely densities – ice, olivine, iron.

There are very little experimental data upon which to base a model that connects micrometeoroid kinetic energy with impact damage diameter in glassy targets, especially that which might be caused by low mass hypervelocity projectiles. Yet, kinetic energy and mass are the given starting points for this study. However, there have been many studies of lunar craters, even close-up examinations of glass-like rocks returned from the Apollo missions. In addition, both U.S. (e.g. LDEF, HST) and European (e.g. Eureca) spacecraft solar panels and other spacecraft exposed components have been returned to the laboratory for impact crater examination.

Figure 9 is a photo of a 30μm diameter impact crater produced in a lunar 'glass-like' rock that was returned by an Apollo lunar mission.[11] It is exhibited here as an example of the kind of

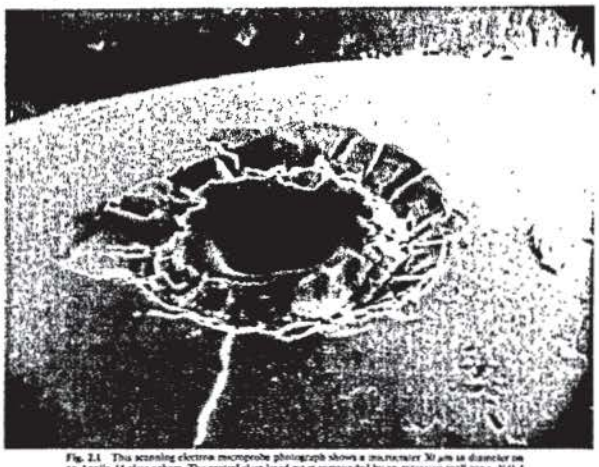

Figure 9 – Photo of a 30μm diameter crater in an Apollo 11 glass sphere returned from the lunar surface. (Ref. 11)

damage that might be inflicted on glass optics by a single hypervelocity micrometeoroid. The crater consists of a central bowl-shaped pit with seriously disrupted wall morphology. The surrounding glass and dielectric coating of the solar window can be expected to be shattered over an area that will be identified in this report as the damage crater or damage area.

Crater Damage Diameter Determined from Micrometeoroid Mass

Laboratory experiments performed by a number of investigators in which high velocity projectiles were fired at glass targets produced the following relation between particle mass and crater damage diameter.[12]

$$\log_{10}D = \log_{10}C + \lambda\log_{10}m \quad \text{.....Eq. (1)}$$

where D is the crater diameter, m is mass, and C and λ are empirically derived constants.

These same experiments have shown that no single value of the empirically derived constants applies equally well to small (~1μm dia.) or large (dia. > 10μm) craters. A density of 3g/cm^3 and a velocity of 20km/s were assumed by the developers of Eq. (1). See Figure 8. Equation (1) was used to calculate an estimated impact crater diameter that was then compared with empirical results from the bombardment of the protected gold mirror target with latex and iron projectiles of known size, mass, and velocity.

Crater Damage Diameter Determined from Micrometeoroid Energy

A.Watts et al. (Ref.13) have constructed a crater impact model derived from LDEF examinations that they have applied to brittle materials. The model predicts crater damage diameter, d_c, in brittle materials as a function of projectile density, ρ_p, target density, ρ_t, projectile velocity, u, and projectile diameter, d_p. These are related in the following equation.

$$d_c = \text{const.}\ (\rho_p/\rho_t)^{0.3333}u^{0.66666}d_p \quad \text{.....Eq. (2)}$$

The const. in the above equation was derived from experimental impact data from aluminum projectiles fired at aluminum targets. The form of the equation is similar to power law empirical relations developed by other investigators.[11,12] For a glassy target, an application of this equation worked best with const. = 10^{-2}. Target density, ρ_t, was chosen as 2.5g/cm^3, the value for BK7 glass. Projectile densities for latex (1.1 gm/cm^3) and iron (8 gm/cm^3) were used to enable a comparison of computed impact crater diameters with empirical results obtained on the gold mirror target.

The results of a comparison of impact crater diameters measured empirically on the gold target mirror and computed from Eqs. (1) & (2) are presented in Table 2 below. A velocity of 10 km/s was used for Eq. (2) as being representative of the experimental latex and iron projectile velocities.

Table 2. A comparison of measured impact crater diameters with diameters computed from proposed analytical formulae.

		Damage Diameter (μm)		
Projectile	**Mass**	**Empirical**	**Equation (1)**	**Equation (2)**
Latex	0.24E-12 g	1.64 ± 0.21	5.3 - 7.9	2.6
Iron	6.7E-12 g	7.36 ±2.49	18.8 - 27.3	8

The agreement among the damage diameters determined empirically and analytically is not perfect, but not bad considering that variations in projectile and target densities and projectile velocities are not fully accounted for in the table. The results at least establish a range of damage sizes, roughly 1.6 μm – 27μm diameter, that are likely to occur from hypervelocity micrometeoroid impact.

Damage area estimates from the empirical results are next used to estimate the degree of scattering to be expected from micrometeoroid impacts.

SURFACE SCATTER EXPECTED FROM MICROMETOROID IMPACTS

The shapes of individual impact craters in a metal surface are depicted in Figs. 5, 6 & 7, and in a glassy surface in Fig. 9. A typical iron hypervelocity projectile impact, produced in the laboratory and dimensioned as shown in Fig. 7, had a damage diameter of 6.6 μm, a pit diameter of 2.2 μm, and a pit depth of ~1.3μm. Generally, surface scattering follows a d/λ^n law, where d is chosen as the crater diameter, λ is the wavelength of incident light, and n varies with the ratio of d/λ. For $\lambda >> d$, a Rayleigh approximation can be used and $n = 4$. When $\lambda \leq d$, as is likely to be the case for the impact dimensions in Table 2 for most space optical systems, a more complete Lorenz-Mie theory should be used to characterize the degree of scattering to be expected from a single crater site. A geometrically diffuse scattering pattern is the likely result of light wave interaction with crater sites similar to those depicted in Figs. 5-7. If impact craters can be considered as a surface roughness, then Spyak & Wolfe (Ref. 14) have published a series of studies in which surface scatter characteristics, such as the bidirectional reflectance distribution function(BRDF) or its transmitting equivalent, the bidirectional transmittance distribution function (BTDF), can be computed from measurements of particulate area coverage and connected quantitatively with Mil Spec contamination levels.

A pragmatic way to deal with this situation for an individual optical surface, when the number of expected impacts should be a small fraction of total area, is to assume that light striking an individual impact crater is diffusely scattered and presumed lost to the system; then determine the percent area coverage (PAC) for N impact sites.

As was stated above, the number of expected hypervelocity impacts varies depending on location in space or seasonal timing in Earth orbit, but is generally expected to be low, as indicated by actual measurements.[1-4] One example of a regional location where high mircrometeoroid density might be encountered is provided by Fig. 3 and the JPL Environmental Requirements Document for a 3 year Mars orbital mission.[9] In order to estimate what impact this environment might have on an exposed optical element, consider the particle fluence, mass, and velocity distribution presented in Fig. 3. It has already been established experimentally and analytically that the least massive particles, 10^{-12} g, either ice-like or iron as extreme density examples, can produce craters

with diameters in the range of 1.6μm to ~ 10μm. An application of Eq. 2 to the data of Fig. 3

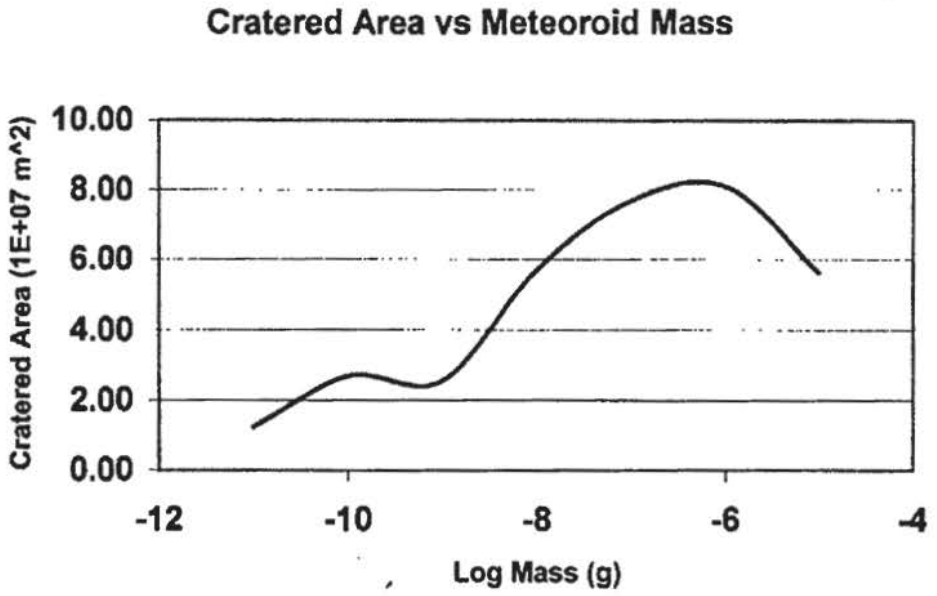

Figure 10. Cratered area as a function of particle mass as would be expected from the fluence, mass, and velocity distribution presented in Fig. 3

produced the cratered area distribution presented in Fig. 10. The total cratered area is computed to be about 34E-7 m^2 for a 3 year exposure. Because this example uses an omnidirectional flux, a shielded element would experience far fewer impacts. Once corrected for an appropriate solid angle exposure, the degree of expected surface scatter, or throughput attenuation , would be just about immeasurably small. For a 1 m^2 target area, the PAC would be 0.0034%. With an average crater diameter of 10μm, as might be expected from particles with mass in the 10^{-12} g range, this PAC converts to about 4000 sites/ft^2, equivalent to a Mil Std 1246C cleanliness level of between 50 and 100.

CONCLUSIONS

Hypervelocity impact craters, produced in a controlled experiment by μm- sized latex (ice-like) projectiles with density 1.1g/cm^3 and by iron projectiles with density ~8g/cm^3, and with velocities in the 10 – 20 km/s range, were dimensioned using SEM and ATF probes. This enabled a direct connection between particle impact energy and crater size for particle sizes, masses, and velocities that resemble those most likely to be encountered in orbits far from Earth. When projectile masses and velocities were inserted into matched analytical models, the computed crater dimensions were in reasonable agreement with those produced experimentally on a gold coated beryllium substrate mirror.

With this bound placed on the accuracy of the analytical models, an expected degree of surface corruption for a selected 3- year Mars orbit meteoroid fluence was computed to be about 0.0034% for a completely exposed 1 m^2 surface area. For an assumed 10μm average crater

diameter, this would convert to a mirror equivalent cleanliness level between 50 & 100 (Mil Std 1246C). A similar procedure could be used to estimate surface damage for another type of meteoroid flux model.

REFERENCES

(1) P. Staubach, et al., "The Meteoroid Environment Near Earth", *Adv. Space Res.*, 19, No. 2, 301-308, 1997.

(2) G. Drolshagen, et al., "HST Solar Array Impact Survey: Revised Damage Laws and Residue Analysis," *Adv. Space Res. Vol. 19, No. 2*, pp. 239-251, 1997.

(3) E.A. Taylor, et al., "Impacts on HST and EuReCa Solar Arrays Compared With LDEF Using A New Glass-to-Aluminum Conversion," *Adv. Space Res. Vol. 23, No.1.* pp. 83-87, 1999.

(4) W.J. Cooke III, in "Natural Environment Near the Sun/Earth-Moon L2 Libration Point", document prepared for the Next Generation Space Telescope program, S.W. Evans, ed., NASA Marshall Space Flight Center.

(5) Jon K. Hillier et al., "Interplanetary dust detected by the Cassini CDA Chemical Analyzer", *Icarus*, 190 (2007) pp. 643-654.

(6) J. B. Heaney, et al., "Hypervelocity particle impact studies performed on a gold-coated beryllium substrate mirror," in SPIE Vol. 5487, Optical, Infrared, and Millimeter Space Telescopes, John C. Mather, ed., Glasgow, Scotland June 2004.

(7) E. Grün, et al., "Collisional Balance of the Meteoritic Complex", *Icarus* 62, 244-272, 1985.

(8) S. Kempf, et al., "Cassini between Earth and asteroid belt: first in-situ charge measurements of interplanetary grains ", *Icarus* 171, 317–335, 2004 .

(9) D.T. Newell, "Mars telecom Orbiter *Preliminary* Environmental Requirements" Document, JPL, 22 July 04.

(10) M. Stübig, et al., "Laboratory simulation improvements for hypervelocity micrometeorite impacts with a new dust particle source", Max Planck Institüt für Kernphysik, Saupfercheckweg 1, D-69117 Heidelberg, Germany, Jan. 31, 2001. (c.f. *Planetary and Space Science,* Vol. 49, pp. 853-858, (2001).

(11) H. J. Melosh, Impact Cratering – A Geologic Process, Oxford Univ. Press, New York, 1989.

(12) F. Hörz, et al. "Lunar Microcraters: Implications For The Micrometeoroid Complex." *Planet. Space Sci., Vol 23*, pp151-172, 1975.

(13) A. Watts, et al., "Optical scatter due to impact effects," SPIE Vol. 1761, p. 73, 1992.

(14) P. R. Spyak and W. L. Wolfe, "Scatter from particulate-contaminated mirrors. Part 4: properties of scatter from dust for visible to far-infrared wavelengths," *Optical Engineering Vol. 31,* p. 1775, Aug. 1992.